24th INTERNATIONAL CONGRESS ON SOUND AND VIBRATION
23–27 July 2017, London

ICSV24
23-27JULY 2017
LONDON CALLING

A HYBRID HIGH-ORDER SLIDING MESH INTERFACE FOR FINITE DIFFERENCE SCHEMES

Ryu Fattah and Xin Zhang
Hong Kong University of Science and Technology, Mechanical and Aerospace Engineering, Clear Water Bay, Kowloon, Hong Kong (S.A.R)
email: meryuf@ust.hk

High-order computational aeroacoustic simulations of complex engineering problems may require the effects of moving boundaries to be resolved. This may be achieved by the immersed boundary method, the over-set grid method, or by a sliding mesh interface. The computational cost associated with a sliding mesh interface is mainly due to the continuous re-evaluation of the interpolation scheme coefficients. These coefficients are evaluated by inverting a non-sparse square matrix, with a size that is based on the interpolation stencil. In this paper the ongoing development of a sliding mesh interface strategy is described that aims to remove the need for re-evaluating the interpolation coefficients. This is achieved by combining patched and sliding interfaces, and the accuracy and the computational cost of this method are discussed.

Keywords: sliding mesh, moving grids

Introduction

High-resolution calculations of compressible fluid flows require low dispersion and low dissipation numerical methods in order to accurately capture the generation, propagation and interactions between the acoustic, vorticity, and entropy waves. If the computational domain is built as block-structured grids then these requirements can be achieved by using high-order and optimized finite differencing schemes. The effect of boundary motion is an additional requirement, for example for simulations of turbo-machinery, and this can be resolved by a deforming mesh [1, 2], sliding mesh [3, 4], or an immersed boundary method [5].

An essential element to each of these methods is the interpolation of data, which must be accurate enough to ensure that the transfer of information is not affected by dissipation or dispersion errors. This can be achieved by using large-stencil, high-order, and wave-number optimized interpolation schemes [6]. Therefore, the overhead computational cost of a high-order moving-boundary simulation may be influenced by the size of interpolation stencil, and the implementation complexity that can lead to a loss in computational efficiency on larger scale computations.

Typically, interpolation schemes have been directly applied to the primitive variables. Therefore, a two-dimensional sliding interface requires a two-dimensional interpolation method. However, if the sliding interface is evaluated in terms of the characteristic fluxes propagating normal to the interface, then the interpolation required for a two-dimensional domain can be performed using a one-dimensional interpolation scheme [3]. Characteristic methods are also useful to provide high-order solutions on block interfaces with a grid discontinuity [7], non-reflective boundary conditions [8, 9], and zonal grid refinement [10, 11]. However, the characteristic method is known to perform less accurately when the flux through the interface is zero [12]. In these situations, a central filtering scheme

that interpolates the primitive variables beyond the block edge can ensure a smooth and continuous solution. This manuscript outlines the development a new sliding mesh strategy that aims to reduce the computational cost and complexity of the method, to ensure a method that is applicable to parallel flows, and to minimise the implementation complexity to maximise the computational efficiency for large scale computations.

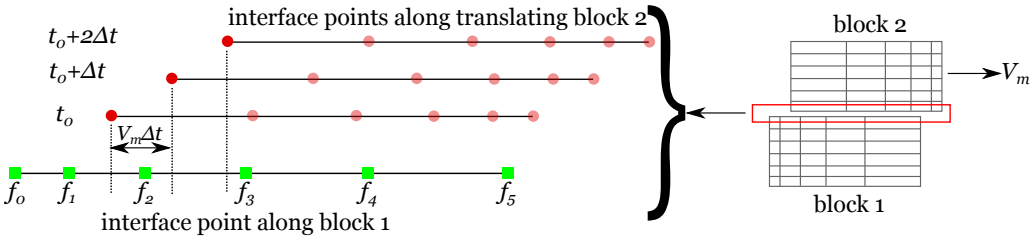

Figure 1: An example of the interpolation scheme progression for a non-uniformly spaced sliding interface.

The potential reductions in the computational cost for a sliding mesh method is outlined with the aid of Figure 1. In Figure 1 the sliding interface is defined between blocks 1 and 2. The grid points along each side of the interface are non-uniformly spaced. As block 2 translates at a mesh translation velocity of V_m, the projection of the grid points of block 2 onto block 1 will change. The interface condition on block 2 requires the data on block 1 at the projected points, and this information is evaluated by an interpolation scheme. The interpolation scheme will vary across the interface, and it will change with every time step, due to the non-uniformity of the grid points.

The number of calculations required to perform the sliding interface condition can be divided into two parts. Firstly, the interface condition requires the interpolation schemes to be applied to every point along the interface, and on both sides of the interface. Secondly, at every subsequent time level, the grid point overlap will be different and require the re-evaluation of the interpolation scheme coefficients. This re-evaluation requires the inversion of a $N_{st} \times N_{st}$ non-spares matrix, where $N_{st}+1$ is the size of the interpolation stencil. Therefore, at every time step a total of $2N_yN_{ss}$ interpolations are required for the interface condition, where N_y is the number of grid points along the interface, and N_{ss} is the number of sub-iterations in the temporal scheme. Additionally $2N_yN_{ss}$ inversions of the non-spare matrix are required at every time step. The size of the interpolation stencil N_{st} must be adequate to resolve the global order of accuracy, and the accuracy will also depend on the patch ratio. For practical cases, a sliding interface on a stretched grid may encounter a range of patch ratios. Peers *et al.* [10] showed that the grid convergence of interpolation schemes with $N_{st} > 7$ will diverge from the order of the spatial scheme as the patch ratio diverges away from unity.

A sliding interface defined by a uniformly spaced grid, can reduce the number of interpolation scheme revaluations from $2N_yN_{ss}$ every time step, to a single calculation. The size of interpolation stencil used along the sliding interface can also be reduced, as the patch ratio will be unit. For practical cases, a secondary patch will be required that projects the flow information from the uniform space to the curvilinear grids. Therefore, additional patched characteristic interfaces are required downstream and upstream of the sliding mesh. However, these calculations are more straightforward and do not require the inversion of a large matrix.

Numerical method

In this section the governing equations, and the characteristic interface conditions are outlined. For simplicity, only key elements are presented. For a full description of these methods, the reader is refered to original references for the characteristic [7], patched [10], and the sliding formulations [3].

Governing equations

In the generalized coordinates, the Euler Equations can be expressed as:

$$\frac{\partial \hat{\boldsymbol{Q}}}{\partial t} + \frac{\partial \hat{\boldsymbol{E}}}{\partial \xi} + \frac{\partial \hat{\boldsymbol{F}}}{\partial \eta} + \frac{\partial \hat{\boldsymbol{G}}}{\partial \zeta} = 0, \tag{1}$$

where conserved variables and the Euler fluxes are given by:

$$\hat{\boldsymbol{Q}} = 1/J[\rho, \rho u, \rho v, \rho w, \rho e_T]^T, \quad J = 1/[x_\xi \left(y_\eta z_\zeta - y_\zeta z_\eta\right) + x_\eta \left(y_\zeta z_\xi - y_\xi z_\zeta\right) + x_\zeta \left(y_\xi z_\eta - y_\eta z_\xi\right)], \tag{2}$$

$$\begin{aligned} \hat{\boldsymbol{E}} &= \left(\xi_x \boldsymbol{E} + \xi_y \boldsymbol{F} + \xi_z \boldsymbol{G}\right), \quad \boldsymbol{E} = [\rho u, \rho u u + p, \rho u v, \rho u w, (\rho e_T + p)u], \\ \hat{\boldsymbol{F}} &= \left(\eta_x \boldsymbol{E} + \eta_y \boldsymbol{F} + \eta_z \boldsymbol{G}\right), \quad \boldsymbol{F} = [\rho u, \rho u v, \rho v v + p, \rho v w, (\rho e_T + p)v], \\ \hat{\boldsymbol{G}} &= \left(\zeta_x \boldsymbol{E} + \zeta_y \boldsymbol{F} + \zeta_z \boldsymbol{G}\right), \quad \boldsymbol{G} = [\rho u, \rho u w, \rho v w, \rho w w + p, (\rho e_T + p)w], \end{aligned} \tag{3}$$

where ρ is the fluid density, (u, v, w) is the velocity, p is the pressure, the total energy density is $e_T = p/\rho(\gamma - 1) + 1/2\,(u^2 + v^2 + w^2)$, and $\gamma = c_p/c_v$ is the ratio of specific heats and taken as 1.4 for air.

Characteristic formulation

The governing equation can be cast in terms of characteristics along ξ as:

$$\frac{\partial \boldsymbol{R}}{\partial t} + \boldsymbol{L} = \boldsymbol{S}, \tag{4}$$

with

$$\begin{aligned} \boldsymbol{L} = \boldsymbol{\Lambda}\frac{\partial \boldsymbol{R}}{\partial \xi}, \quad \partial \boldsymbol{R} = \boldsymbol{P}^{-1}\partial \boldsymbol{Q}, \quad \boldsymbol{\Lambda}\frac{\partial \boldsymbol{R}}{\partial \xi} = \boldsymbol{P}^{-1}\left(\xi_x \frac{\partial \boldsymbol{E}}{\partial \xi} + \xi_y \frac{\partial \boldsymbol{F}}{\partial \xi} + \xi_z \frac{\partial \boldsymbol{G}}{\partial \xi}\right), \\ \boldsymbol{S} = -J\boldsymbol{P}^{-1}\left[\frac{\partial \hat{\boldsymbol{F}}}{\partial \eta} + \frac{\partial \hat{\boldsymbol{G}}}{\partial \zeta} + \boldsymbol{E}\frac{\partial}{\partial \xi}\left(\frac{\xi_x}{J}\right) + \boldsymbol{F}\frac{\partial}{\partial \xi}\left(\frac{\xi_y}{J}\right) + \boldsymbol{G}\frac{\partial}{\partial \xi}\left(\frac{\xi_z}{J}\right)\right]. \end{aligned} \tag{5}$$

where, $\boldsymbol{P}\boldsymbol{\Lambda}\boldsymbol{P}^{-1}$ is the flux Jacobian along ξ, and $\boldsymbol{P}$ and $\boldsymbol{P}^{-1}$ are the left and right eigenvectors of the flux Jacobian. The flux derivatives along a block interface can be expressed as characteristic fluxes through a surface defined by $\nabla\xi = \text{const}$. Based on this formulation, boundary conditions, and interface conditions for both static and sliding interfaces can be defined.

Characteristic interface conditions

The condition that $\partial \boldsymbol{R}/\partial t$ is continuous across the block interface is satisfied by upwinding the charactersitc information according to its eigenvalue:

$$(L_i^*)^L = L_i^R - S_i^R + S_i^L, \quad \text{if} \quad \lambda_i^L = \lambda_i^R < 0 \tag{6}$$

$$(L_i^*)^R = L_i^L - S_i^L + S_i^R, \quad \text{if} \quad \lambda_i^L = \lambda_i^R > 0 \tag{7}$$

The extension of this method to non-conformal grids is achieved by interpolating the characteristic fluxes and source terms across the non-conformal space [11, 10] by an interpolation scheme. Finally, the extension of patched interfaces to a sliding interface additionally requires the characteristic fluxes to be evaluated in a reference frame that follows the local block [3]. The latter, requires additional flux corrections to account for the effect that the mesh translation has on the characteristic fluxes.

Hybrid patched and sliding interface

The proposed sliding mesh strategy is illustrated in Figure 2, and is outlined as follows. Firstly the sliding region is locally remeshed as a uniform grid and secondly, the transition from the uniform grid to the curvilinear space is imposed by a patched interface condition. By this method, the number of interpolation scheme re-evaluations is set to a single calculation, at every instance that the mesh is translated.

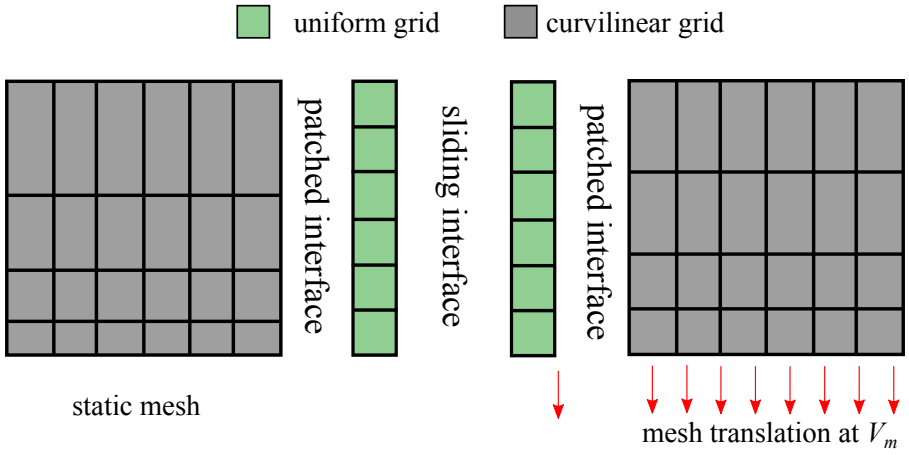

Figure 2: Schematic of the hybrid uniform sliding interface method.

As the mesh translates, the central points to the interpolation scheme will change with time. By setting the mesh displacement to be some factor of the local grid spacing, the central points of the interpolation scheme can be easily updated. This is achieved by setting the mesh translation V_m as:

$$V_m = \frac{\Delta y}{N_m \Delta t}, \tag{8}$$

where Δy is the uniform grid spacing, N_m is an integer number that specifies the number of time steps required for the mesh to translate by Δy, and Δt is the time step size.

Results

Two benchmark problems are evaluated for the validation of the sliding interface method. The first is an acoustic pulse propagating over a uniform base flow, and the second is an isentropic vortex convecting across a uniform base flow. Results obtained by various hybrid sliding interfaces are obtained and compared to a solution obtained by a fixed grid. The domain size for both cases is $0 < x < 4$ meters, and $0 < y < 3$ meters. The domain is divided into four evenly sized blocks with a length of 1m and a height of 3m. The sliding interface is defined along $x = 2$ and the patched interfaces are along lines at $x = 1$ and $x = 3$. The base flow for both cases is uniform and set to a Mach number of $M_\infty = 0.5$.

The Euler fluxes are evaluated by high-order spatial schemes [13], and the fluxes are corrected along the patched and sliding interfaces by a characteristic method. The solution is advanced to the next time level using high-order order Runge-Kutta method [14] with and time step set to ensure CFL< 0.5. At the end of each time step, the solution is modified by a high-order filter [15] and the primitive variables along the characteristic interfaces are treated using a 6th order explicit central filter [16].

Acoustic pulse across a sliding interface

A sinusoidal acoustic monopole forcing defined by Bailly and Juve [17] is placed near the centre of the computational domain. The acoustic properties of the forcing are set to $\epsilon = 0.05$, $(x_0, y_0) = (1.25, 1.5)$, $\omega = 15$, $\alpha = ln(2)/0.01$, according to the parameters defined in [17]. The instantaneous pressure fields from three grids, with varying patch ratios, are illustrated in Figure 3. This figure also includes close-up views of the patched interface region. Figure 4 illustrates the instantaneous pressure field taken along a line at $y = 2$, and recorded at a non-dimensional time of $t = 1.25$. Several cases with different patch ratios, and mesh translation speeds are shown, and the results show that there is no discernible effect of the sliding interface or the patched interface on the acoustic pulse propagation.

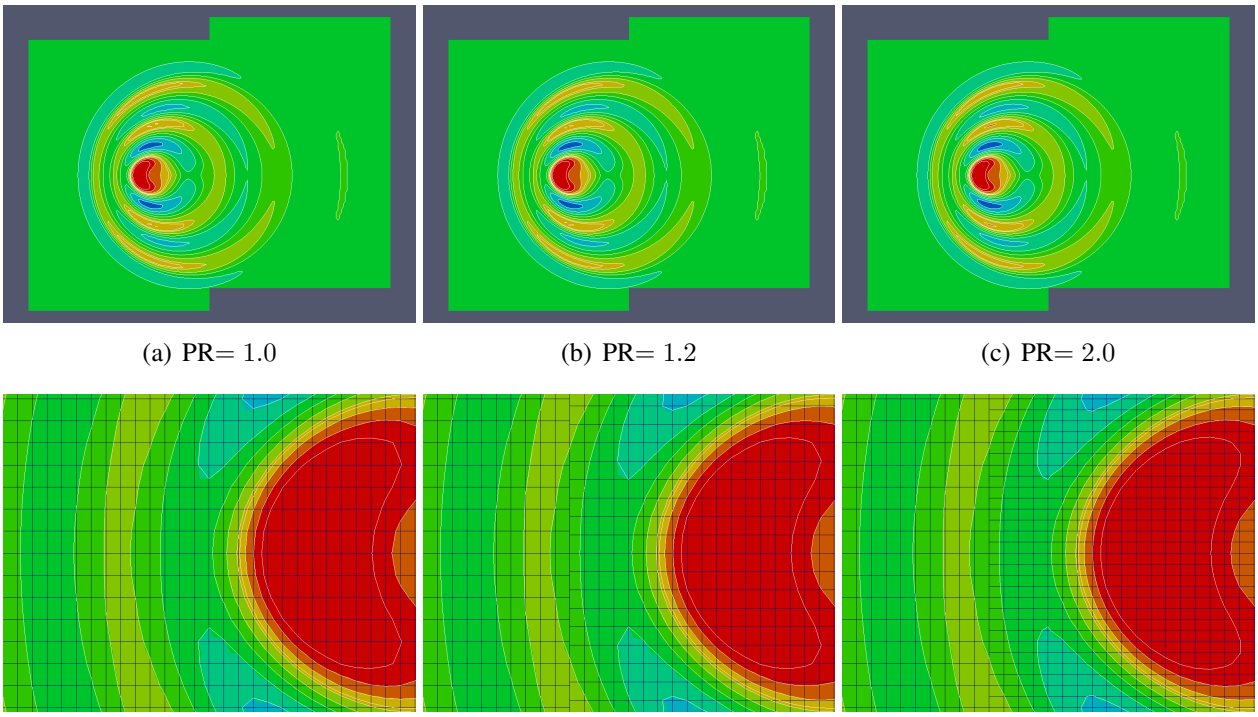

(a) PR= 1.0 (b) PR= 1.2 (c) PR= 2.0

(d) PR= 1.0 closeup (e) PR= 1.2 closeup (f) PR= 2.0 closeup

Figure 3: Disturbance density field induced by an acoustic source, solved by grids of varying patch ratios (PR), and at a constant mesh translation speed of $V_m = 0.1$. The contour levels range from $-3 \times 10^{-2} < \rho' < 3 \times 10^{-2}$ across 10 levels.

Vortical wave across a sliding interface

The effects of the patched and sliding interfaces on the convection of an isentropic vortex are studied in this section. The flow field with a two-dimensional vortex is defined by [18] as:

$$\psi = \frac{\epsilon}{2\pi}\sqrt{\exp\left[1 - \left((x - x_0)^2 + (y - y_0)^2\right)/L^2\right]}, p = p_\infty \left(\rho/\rho_\infty\right)^\gamma \tag{9}$$

$$\rho' = \rho_\infty \left[1 - \frac{\gamma - 1}{2}\psi^2\right]^{\frac{1}{\gamma - 1}}, u' = \frac{y - y_0}{L}\psi, v' = -\frac{x - x_0}{L}\psi, \tag{10}$$

The instantaneous transverse velocity is shown in Figure 5 from three cases with different patch ratios, and the transverse velocity profile taken along the centreline at a time of $t = 3$ along Figure 6

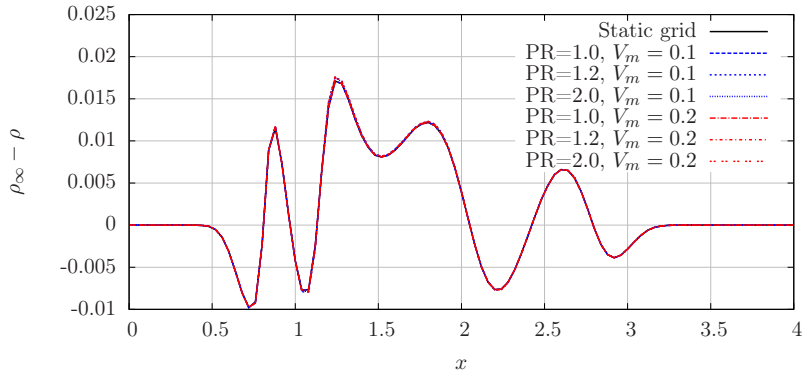

Figure 4: Acoustic pressure distribution along $y = 2$ and $0 < x < 4$ from grids with various patch ratios (PR) and mesh translation speeds (V_m).

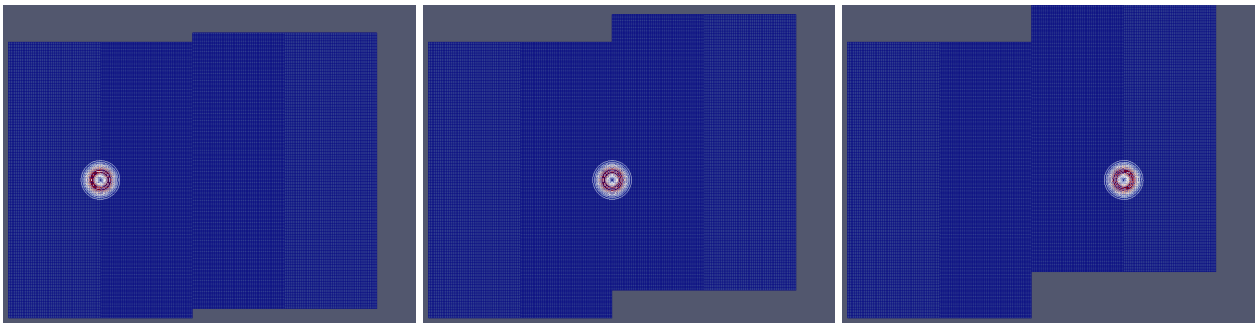

(a) $t = 1$ (b) $t = 2$ (c) $t = 3$

Figure 5: Disturbance transverse velocity field induced by vorticity convection, solved on a grid with a patch ratio of (PR$= 2$), and at a mesh translation speed of $V_m = 0.2$. The contour levels range from $-1 \times 10^{-5} < \rho' < 1 \times 10^{-5}$ across 10 levels.

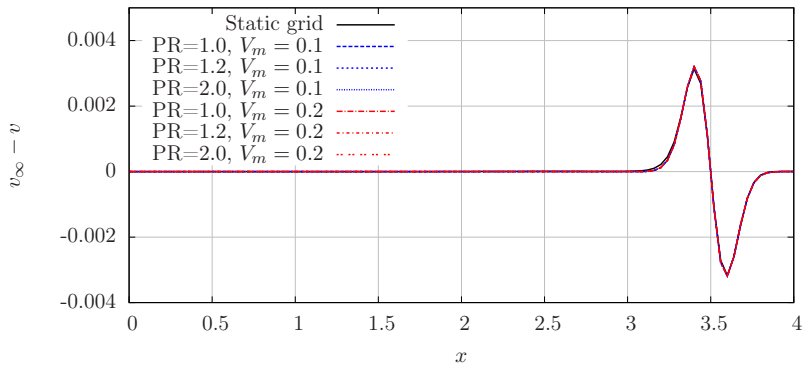

Figure 6: Transverse velocity distribution along the the vortex core streamline, from grids with various patch ratios (PR) and mesh translation speeds (V_m).

Computational cost

The computational time required to perform the acoustic pulse test case was measured for the monopole benchmark case, using a patch ratio of 1. For this case the patched interface can be treated as a one-to-one boundary, and the overhead computational costs from the sliding interface, the patched interface, and the re-evaluation of interpolation coefficients, can be measured.

Configuration	CPU time increase %	Description
Sliding interface	N/A	No patched interface, no re-evaluation, no ghost points
Hybrid interface	14%	Patched and sliding interfaces, with 3, or 5 ghost points
Sliding interface	14%	Re-evaluation of interface points only
Sliding interface	27%	Re-evaluation of interface points and 3 ghost points
Sliding interface	48%	Re-evaluation of interface points and 5 ghost points

Table 1: Computational run times of various sliding interface methods.

The results outlined in Table 1 shows that the re-evaluation of the interpolation scheme coefficients (with $N = 5$), adds 13% to the simulation time. With the use of a central filter across the interfaces regions, the ghost point data must be evaluated. Re-evaluation of the interpolation coefficients for more ghost points add significantly greater computational cost. The results obtained here are for an interpolation scheme with a stencil size of $N = 5$. However, if a larger stencil is used (to ensure greater accuracy on more extreme patched grids), then the overhead cost of the re-evaluation can be expected exceed the cost induced by the patched interfaces. Finally, the implementation simplicity of a sliding interface on a parallel computation is more simple and straightforward on a uniformly spaced grid.

Conclusion

An overview of the ongoing development of a sliding mesh strategy based on characteristic interfaces is given in this paper. The method employed to resolve the effects of a moving boundary uses high-order finite differencing and an interface condition that induces minimal errors to the hydrodynamic and acoustic disturbances in the computational domain. The method employed relies on combining patched and sliding interface conditions that are formulated in terms of characteristics. These conditions work well, unless the flow is parallel to the interface edge. Under such conditions, a central filter with interpolated ghost points can be used to overcome the inaccuracies induced by the interface condition.

The computational cost associated with the re-evaluation of interpolation scheme coefficients is removed by employing a patched interface, and a sliding interface across a uniform grid. This has two advantages. Firstly, it greatly simplifies the implementation procedure, and secondly, it can reduce the computational cost for cases with interpolation schemes with $N > 5$, or cases that require ghost point interpolation. The method has been verified under several configurations on two benchmark problems, and the results demonstrate that the interface conditions, and the mesh translation, do not induce any discernible errors to the solution.

References

1. J. Stephens, B. A. Robinson, H. T. Y. Yang, and J. T. Batina, "Aeroelastic analysis of wings using the Euler equations with a deforming mesh," *Journal of Aircraft*, vol. 28, no. 11, pp. 781–788, 1991.

2. N. C. Prewitt, D. M. Belk, and W. Shyy, "Parallel computing of overset grids for aerodynamic problems with moving objects," *Progress in Aerospace Sciences*, vol. 36, pp. 117–172, 2000.

3. R. Johnstone, L. Chen, and R. D. Sandberg, "A sliding characteristic interface condition for direct numerical simulations," *Computers and Fluids*, vol. 107, pp. 165–177, 2015.

4. J.-m. Gagnon, G. D. Ciocan, C. Deschenes, and M. Iliescu, "Numerical and experimental investigation of rotor-stator interactions in an axial turbine : numerical interface assessement," *Proceedings of the ASME Fluids Engineering Division Summer Meeting*, no. FEDSM2008-55183, 2008.

5. E. Balaras, "Modeling complex boundaries using an external force field on fixed Cartesian grids in large-eddy simulations," *Computers and Fluids*, vol. 33, no. 3, pp. 375–404, 2004.

6. C. K. W. Tam and K. a. Kurbatskii, "A wavenumber based extrapolation and interpolation method for use in conjunction with high-order finite difference schemes," *Journal of Computational Physics*, vol. 157, no. 2, pp. 588–617, 2000.

7. J. W. Kim and D. J. Lee, "Characteristic interface conditions for multiblock high-order computation on singular structured grid," *AIAA Journal*, vol. 41, no. 12, pp. 2341–2348, 2003.

8. J. Gill, R. Fattah, and X. Zhang, "Towards an effective non-reflective boundary condition for computational aeroacoustics," *Journal of Sound and Vibration*, vol. 392, pp. 217–231, 2017.

9. R. J. Fattah, J. R. Gill, and X. Zhang, "Towards a Generic Non-Reflective Characteristic Boundary Condition for Aeroacoustic Simulations," *AIAA 2016-2914*, 2016.

10. E. Peers, X. Zhang, and J. W. Kim, "Patched characteristic interface condition for high-order multiblock aeroacoustic computation," *AIAA Journal*, vol. 48, no. 11, pp. 2512–2522, 2010.

11. T. Sumi, T. Kurotaki, and J. Hiyama, "Interpolated characteristic interface conditions for zonal grid refinement of high-order multi-block computations," *International Journal of Computational Fluid Dynamics*, vol. 26, no. 1, pp. 37–41, 2012.

12. Y. Du and P. J. Morris, "A new block interface condition for aeroacoustic applications," *AIAA 2013-2210*, 2013.

13. J. W. Kim and R. D. Sandberg, "Efficient parallel computing with a compact finite difference scheme," *Computers & Fluids*, vol. 58, pp. 70–87, 2012.

14. F. Hu, M. Hussaini, and J. Manthey, "Low-dissipation and low-dispersion Runge-Kutta schemes for computational acoustics," *Journal of Computational Physics*, vol. 124, pp. 177–191, 1996.

15. J. W. Kim, "High-order compact filters with variable cut-off wavenumber and stable boundary treatment," *Computers & Fluids*, vol. 39, no. 7, pp. 1168–1182, 2010.

16. O. V. Vasilyev, T. S. Lund, and P. Moin, "A general class of commutative filters for LES in complex geometries," *Journal of Computational Physics*, vol. 146, no. 1, pp. 82–104, 1998.

17. C. Bailly and E. C. D. Lyon, "Linearized Euler Equations," *AIAA Journal*, vol. 38, no. 1, pp. 22–29, 2000.

18. H. Yee., N. Sandham., and M. Djomehri., "Low-Dissipative High-Order Shock-Capturing Methods Using Characteristic-Based Filters," *Journal of Computational Physics*, vol. 150, no. 1, pp. 199–238, 1999.